HHS Public Access

Author manuscript

Nat Commun. Author manuscript; available in PMC 2014 July 01.

Published in final edited form as:

Nat Commun. 2014 ; 5: 3009. doi:10.1038/ncomms4009.

Structure-based mechanism for Na^+/melibiose symport by MelB

Abdul S. Ethayathulla[1], **Mohammad S. Yousef**[1,†], **Anowarul Amin**[1], **Gérard Leblanc**[2,‡], **H. Ronald Kaback**[2], and **Lan Guan**[1,*]

[1]Department of Cell Physiology & Molecular Biophysics, Center for Membrane Protein Research, Texas Tech University Health Sciences Center, Lubbock, TX, 79430, USA.

[2]Department of Physiology, University of California, Los Angeles, CA 90095, USA.

Abstract

The bacterial melibiose permease (MelB) belongs to the glycoside-pentoside-hexuronide:cation symporter family (GPH), a part of the major facilitator superfamily (MFS). Structural information regarding GPH transporters and other Na^+-coupled permeases within MFS has been lacking, although a wealth of biochemical and biophysical data are available. Here we present the 3D crystal structures of *Salmonella typhimurium* $MelB_{St}$ in two conformations, representing an outward partially occluded and an outward inactive state of $MelB_{St}$. MelB adopts a typical MFS fold, and contains a previously unidentified cation-binding motif. Three conserved acidic residues form a pyramidal-shaped cation-binding site for Na^+, Li^+, or H^+, which is in close proximity to the sugar-binding site. Both co-substrate-binding sites are mainly contributed by the residues from the N-terminal domain. These two structures and the functional data presented here provide mechanistic insights into Na^+/melibiose symport. We also postulate a structural foundation for the conformational cycling necessary for transport catalyzed by MFS permeases in general.

Introduction

Membrane transport proteins from the glycoside-pentoside-hexuronide:cation symporter family[1,2] (GPH, TC 2.A.2; Supplementary Fig. S1a, b) are widely found in all life forms, and *Escherichia coli* MelB ($MelB_{Ec}$) is the best-studied representative. However, our

*Corresponding author. Lan.Guan@ttuhsc.edu.

†Current address: Department of Physics, College of Arts & Sciences, Southern Illinois University, Edwardsville, IL 62026-1654 (On leave from: Biophysics Department, Faculty of Science, Cairo University, Egypt).

‡Current address: CEA-DSV- Fontenay aux Roses, Cross Division of Toxicology, 92 265 Fontenay aux Roses BP 6 France.

Author Contributions

ASE, MSY, and LG performed protein production, crystallization, X-ray diffraction, data collection and processing. ASE and LG performed collection and processing of data for the PDB accessing 4M64 and structure interpretation. LG, ASE, and AA designed and AA performed all transport assays and FRET measurements. LG interpreted functional data. LG directed the research. HRK and GL provided advice and research reagents. All authors contributed to manuscript preparation. LG and ASE wrote the manuscript with help from HRK.

Conflict of interest

The authors declare no conflict of interest.

Accession codes

The protein coordinates and structure factor have been deposited in the Protein Data Bank with the accession number 4M64.

Supplementary Information is available.

understanding of transport mechanisms with these important permeases is limited by lack of high-resolution structures. *Salmonella typhimurium* MelB ($MelB_{St}$) has more than 85% primary sequence identity with $MelB_{Ec}$[3,4], and both proteins exhibit about 54% similarity with the human major facilitator superfamily (MFS) domain-containing Protein 2A (MFSD2A); moreover, the residues essential for transport in MelB are functionally conserved in MFSD2A[5]. Remarkably different from other MFS transporters[6], MelB catalyzes electrogenic symport of galactosides with Na^+, Li^+, or H^+[7]; the broad cation selectivity is a prominent feature. Some MelB orthologues selectively couple sugar symport with one or two out of the three cations, but the anomeric configuration of the sugar is important with respect to specific coupling cations[7]. For instance, sugars in the α-configuration (melibiose and raffinose) utilize all three cations, but β-anomers of galactopyranosides couple only to Na^+ and Li^+ [8].

$MelB_{St}$ shares similarity with regard to cation-coupling specificity and other transport features with the well-studied $MelB_{Ec}$[4,7,9-12]. All three coupling cations compete for a single binding site with a protein/sugar/cation stoichiometry of unity[4,13,14]. Electrogenic sugar symport is driven by $\Delta\tilde{\mu}_{H+,Na+,orLi+}$ depending on the coupling cation[4]. Thermodynamically, MelB transduces the free energy from the downhill translocation of a cation to drive translocation of sugar against a concentration gradient, and vice versa[4,12].

Here, we present 3D X-ray crystal structures of $MelB_{St}$ in two distinct conformations, refined to 3.35 Å. The structure is in general agreement with the predicted model of MelB[15]. Notably, most MFS members are either H^+ symporters or uniporters. Among the members with solved structures[16-23], $MelB_{St}$ is the sole member that utilizes Na^+ primarily as a coupling cation for symport, and uses a previously uncharacterized coupling mechanism.

Results

Functional characterization

Purified $MelB_{St}$ is monodisperse, stable (Supplementary Fig. S2, a and b) and binds melibiose, 2'-(N-dansyl)aminoalkyl-1-thio-β-D-galactopyranoside (D^2G), or methyl-β-D-thiogalactoside (TMG), but has no affinity for sugars without a galactopyranosyl moiety (Fig. 1a). A single sugar-binding site was determined by Isothermal Titration Calorimetry (ITC) (Fig. 1b, c). Melibiose binding is exothermic with K_d of ~1 mM in the presence of Na^+ or Li^+, which is consistent with previous results[4]. Furthermore, sugar binding is driven energetically by a small favorable enthalpy change (ΔH) and a bigger increase in entropy (TΔS).

Overall fold of $MelB_{St}$

The structure of $MelB_{St}$ was solved by molecular replacement and refined to a resolution of 3.35 Å (Table 1). The asymmetric unit contains four molecules (Mol-ABCD; Supplementary Fig. S3a,b) with twinning and pseudo-translation symmetries. Surprisingly, twinned Mol-B and Mol-D have a conformation different from Mol-A and Mol-C (Fig. 2 and Supplementary Fig. S4a, b). We describe only Mol-A and Mol-B here as representative structures.

As predicted[15], $MelB_{St}$ adopts a typical MFS fold, organized in N- and C-terminal six transmembrane α-helix bundles (Fig. 2) with a connecting cytoplasmic central loop containing two short helices (CH_1 and CH_2), and the cytoplasmic C-terminal tail with another short α-helix (CH_3). Both the N and C termini are on the cytoplasmic side of the membrane, and the overall shape is consistent with the electron-microscopic map of $MelB_{Ec}$[24]. The N- and C-terminal domains are related by a pseudo 2-fold symmetry axis perpendicular to the membrane plane and separated from each other by an internal cavity facing the periplasm. Within each domain, there is two-fold inverted pseudo-symmetry between helices I-III and IV-VI, as well as VII-IX and X-XII, forming repeats A-D (Supplementary Fig. S4c). Like other MFS members[16,18,25], MelB may have evolved from triple-helix repeats with a similar genetic origin.

Most $MelB_{St}$ helices are irregular with kink(s) and tilts (Fig. 2b and Supplementary Figs. S3 and S4). Two to three broken helices are observed in both molecules; helices IV, X, and XI in Mol-A and helices II, VII and X in Mol-B. Mol-A exhibits a periplasmic-facing conformation with a partially occluded internal cavity, due to the interactions between helices I and VII in the N- and C-terminal domains, respectively. This structure is described as an outward partially occluded conformation (Figs. 2a and 5). The cavity is closed on the cytoplasmic side by inter-domain contacts between inner helices IV/X, V/VIII and II/XI; solvent is accessible from the periplasmic side. Mol-B has a partial outward opening compared to fully opened FucP[20], and is described as a partial outward conformation (Figs. 2a and 5). The RMSD between Mol-A and Mol-B is 2.7 Å, and the major differences are found in the first two helices of each repeat (Supplementary Fig. S4c), indicating that the inner helices move relatively independently between the two conformations.

Viewed from the periplasmic side, the internal cavity in Mol-A has an asymmetric charge distribution (Fig. 3a). Except for Lys377 in the C-terminal domain, all other charged residues, including Asp residues (19, 55, 59, and 124), Lys18 and Arg residues (52 and 149), are in the N-terminal domain. The calculated omit maps do not reveal interpretable densities for either bound sugar or cation.

The cation-binding site

A cluster of Asp residues at positions 55 and 59 (helix II), and 124 (helix IV) forms a pyramidal-shaped pocket in Mol-A (Fig. 3a and Supplementary Fig. S5a). In close proximity, there are Tyr120, Thr121 (helix IV) and Thr373 (XI). Together these residues could form the trigonal bipyramid geometry required for a metal-binding site[26,27]. Thr121 forms H-bonds with Asn58 and Asp59, stabilizing the interaction between helices II/IV, and Lys377 H-bonds with Tyr120 separating the negatively charged pocket from the central water-filled cavity (Fig. 3a). Asp124 is buried between Tyr120 and Trp128. Asp59 is buried in a hydrophobic environment (Supplementary Fig. S5c).

Remarkably, Cys replacement at position 55, 59, 124, 58, or 121 differentially alters cation selectivity. Thus, the D55C mutant in $MelB_{St}$ retains only a low level of H^+-coupled melibiose binding and active transport (Fig. 3c, d, and Supplementary Fig. S6a), but Na^+ or Li^+ does not stimulate either binding or transport. The D59C and D124C mutants bind ligand, with reduced affinity (Fig. 3d), but do not catalyze active melibiose transport (Fig. 3c

and Supplementary Fig. S6a). Reduced rates of melibiose efflux and exchange are observed with mutant D59C, but mutant D124C does not exhibit exchange activity. In contrast to WT, melibiose binding, efflux and exchange in the D59C mutant are not stimulated by Na^+ or Li^+ nor is efflux inhibited at acidic pH (Fig. 4); thus, the D59C mutant behaves like a sugar uniporter. None of these mutations has an adverse effect on protein expression (Supplementary Fig. S6b). Furthermore, both the N58C and T121C mutations selectively inhibit H^+- and Na^+-coupled activity, with little effect on Li^+-coupled melibiose transport (Fig. 3c and Supplementary Fig. S6a). Combined with the observed geometry and functional data presented here and elsewhere[7,28-30], we propose that the cation-binding site selectively coordinates Na^+, Li^+ or H_3O^+ through a dynamic change in size and shape[27] dictated by the orientation of Asp55, Asp59, and Asp124. This supports the conclusion that all coupling cations in MelB compete for a single binding site[4,13,14]. It is apparent that each Asp residue at these positions has a specific role in cation binding and coupling. All three Asp residues are required for Na^+ or Li^+ binding, and Asp59 is essential for H^+ binding. Asp59 is buried in a hydrophobic environment (Supplementary Fig. S5c); based on the PROPKA prediction[31], it has a largely elevated pKa of 9.0. We propose that Mol-A is in a protonated state. Since the cation-binding site binds H^+, Na^+, or Li^+ mutually exclusively[4,13,14], a bound Na^+ is not expected in this configuration.

In Mol-B, the pyramidal-shaped cation-binding site is deformed. Displacement of the helix XI kink between helices II and IV places Asp55 and Asp59 in a different environment (Fig. 3b and Supplementary Fig. S5d), distorting the pyramidal arrangement. The deformation of the cation-binding site is probably necessary in order to release the bound Na^+. This conformational change, which is involved in rearrangement of the helices, is expected to contribute to the rate-limiting step of transport[4,9,32]. In this state, Arg52 holds helix XI by H-bonding with backbone atom of Gly378, indicating a primary structural role. Furthermore, Asp55 also stabilizes packing between helices II and XI.

The known crystal structures of other Na^+-coupled symporters[26,33,34] have a relatively low-affinity Na^+-binding motif, where 4-6 partial charges coordinate Na^+. In contrast, MelB utilizes three Asp residues representing a unique, higher-affinity Na^+-binding motif [4,29].

The sugar-binding site

The sugar specificity of $MelB_{St}$ is highly selective for di- or tri-saccharides containing a D-galactopyranosyl moiety or the monosaccharides D-galactose, as in $MelB_{Ec}$[8] or LacY[35-37]. In close proximity to the cation-binding site, a water-filled cavity is observed between residues Asp19 (helix I), Arg149 (helix V), Tyr120, Asp124, and Trp128 (helix IV), as well as Lys377 (helix XI) (Fig. 3a). Asp19 and Arg149 form a salt-bridge on one side of the cavity; Tyr120 and Lys377 are H-bonded on the other side. Cys replacement at each of these positions abolishes or markedly decreases binding, as measured by Trp→D^2G fluorescence resonance energy transfer (FRET), and melibiose transport (Fig. 3c, d and Supplementary Figs. S6, S7), although mutant K377C retains 30-40 % of WT symport activity with each cation (Fig. 3c and Supplementary Fig. S6a). In $MelB_{Ec}$, single-Cys mutation of Asp19 selectively abolishes sugar binding with little effect on Na^+ binding[30], mutant W128F has decreased affinity for 4-nitrophenyl-α-D-galactopyranoside[38], and mutants Y120F and

D124E exhibit decreased sugar- and Na^+-binding affinities[39]. Therefore, these charged or polar side chains, particularly Asp19 and Arg149, play critical roles in sugar selectivity and affinity, and the aromatic residues Trp128 and Tyr120 may contribute to affinity by CH/pi interactions with the pyranosyl ring of the sugar[40,41]. Clearly, a crystal structure with bound sugar is required to determine the sugar-binding coordinates precisely. In Mol-B, the salt bridge between Asp19 and Arg149 is broken, and Trp128 is also displaced from the cavity, suggesting deformation of the sugar-binding site (Fig. 3b). It is noteworthy that the cation-binding site is also collapsed in this conformation, so the Mol-B probably represents an inactive state of $MelB_{St}$.

It is interesting that both LacY and MelB have similar sugar specificity and location of the sugar-recognition sites[35]; however, their cation-binding sites are related by a pseudo two-fold symmetry axis perpendicular to the membrane plane. The location of the Na^+-binding site in MelB is away from Arg149, which is involved in sugar binding, thereby allowing the presence of a strongly negatively charged metal-binding site without a negative influence on sugar binding.

Positive cooperative binding between the co-substrates is well established in MelB[4,38,39,42]. Helix IV, in the middle of the N-terminal domain, physically connects both co-substrate sites. In addition to Tyr120 and Asp124, Lys18 (Fig. 3c and Supplementary Fig. S6) H-bonds with the backbone atom of Met123 (Fig. 3a, b) which links helices I to IV, underscoring the crucial role of helix IV in cooperative binding and transport. Based on the structures, we anticipate that Na^+ binding leads to movement of helix IV, which recruits Asp124, optimizing the pyramidal shape of the cavity with Asp55 and Asp59 and aligning Tyr120 and Trp128 for aromatic stacking with the sugar, thereby increasing affinity. It is well documented that sugar affinity is increased by more than 3 fold in the presence of Na^+ or Li^+[4,13,29,30,43]. Asp124 is required for the completion of the Na^+-binding site[30]

Ionic locks and conformational cycling

Both conformers are present in the same crystal, indicating that $MelB_{St}$ has multiple conformations. Available crystal structures show MFS permeases in inward- or outward-conformations with occluded or partial to fully open cavities (Fig. 5), implying that an individual transporter may favor few conformers within a conformational cluster depending upon the lowest free-energy state. The energy barrier for altering conformational equilibrium between inward and outward clusters may be the formation of an occluded intermediate state. Here we show that extra-membrane electrostatic interactions play a crucial role in this regard.

Both inside-closed structures of $MelB_{St}$ exhibit multiple hydrophobic interactions (hydrophobic patches) on the cytoplasmic side of the transmembrane helices sealing the cavity between N- and C-domains (Fig. 6a). This sealed dynamic domain is also stabilized by inter-domain electrostatic interactions, designated as ionic locks, involving three Arg residues: Arg295 (cytoplasmic end of helix IX), Arg141 (cytoplasmic end of the helix V), and Arg363 (flexible $loop_{10\text{-}11}$) (Fig. 6a, b). At the first ionic lock (L-1), Arg295 forms multiple H-bonds with Gln143 (helix V) and Pro287 (helix VIII) to hold helix V close to the C-terminal domain. At L-2, Arg141 forms four H-bonded ion pairs with Asp351 and

Asp354 (helix X), stabilizing helix X. At L-3, Arg363 ($loop_{10-11}$) forms one ion-pair and two H-bonding interactions with the backbone atoms of Val204, Asp208 (N-terminal side of central $loop_{6-7}$) and Gly74 ($loop_{2-3}$), holding the N-terminal domain in an outward-facing conformation. It is likely that by stabilizing helix X, ionic locks L-1 and L-2 facilitate interaction of Arg363 with its partners. Replacing Arg363, Arg141, or Arg295 individually with Cys yields conformationally compromised mutants that fail to transport but retain affinity for both co-substrates (Fig. 6c, d and Table 2). As indicated from a thread model of $MelB_{St}$ at an inward-facing conformation (Fig. 6a), all three cytoplasmic inter-domain locks are at unlocked state since the residues involved in these electrostatic interactions are 20 Å far apart. Therefore, these three ionic locks play important role in facilitating the formation of outward-facing conformation. On the periplasmic side, Asp35 (helix I) organizes L-4 (Fig. 6a, b) by forming a salt bridge with Arg175 (helix VI) and stabilizes the outward-facing conformation.

Discussion

Similar ionic lock interactions are present in other MFS structures (Fig. 5 and Supplementary Fig. S8). From top to bottom in the Fig. 5, conformations are depicted from the full inward to the full outward states[17,18,20-23,44-46]. None of the predicted locks L-1, L-2, and L-3 exists in cluster-1, which includes the full and partially inward states. L-1 is formed in cluster-2, the inward partially occluded state. When the conformation reaches a more occluded state (cluster-3), both L-1 and L-2 are observed. L-3 is not observed in any of the inward conformers, but exists in most outward structures (cluster-4). Thus, formation of an occluded state likely requires L-1 and L-2, and the outward state requires all three ionic locks. Reverse order of lock formation is expected for the conformational changes to proceed in the opposite direction. The formation and deformation of these ionic interactions are the structural foundation for the function-required conformational switching between inward and outward conformers.

What triggers the locking/unlocking processes? In MelB, the salt-bridge between Arg149 and Asp19 is involved in sugar binding. It is noteworthy that a short cytoplasmic stretch of helix V (Arg141-Arg149) links the sugar-binding site with two ionic locks (L-1 and L-2) (Fig. 6a, b) and also contains two other conformationally important residues, Glu142[42] and Pro148[47]. We propose that sugar binding promotes a dynamic state of the cytoplasmic stretch of helix V (Fig. 6a, b) and triggers locking/unlocking processes associated with a cascade of structural rearrangements for reorientation of the sugar-binding pocket.

We previously proposed a sequential binding kinetic model to explain reversible cation/melibiose symport in MelB based on an alternating-access mechanism (Fig. 7)[9,12,42]. The structural and functional studies discussed here allow integration of the conformational states with kinetic steps in the proposed model for explaining melibiose/Na^+ symport reactions. Although melibiose/Na^+ efflux is explained for experimental simplicity[4], influx is the reverse reaction starting from the intermediate **[6]** (Fig. 7) and proceeds via the red arrows around the circle; active melibiose transport driven by $\Delta\tilde{\mu}_{H+,Na+,orLi+}$ likely occurs in similar fashion. The polarity of transport is controlled by the direction of the net free

energy stored in the form of either the sugar gradient or the electrochemical gradient of Na^+, Li^+ or H^+, and the transport process is reversible.

This simplified scheme for melibiose efflux involves eight states (Fig. 7, *black arrows*): **[1]** *Inward Na^+-bound state*. Binding of a Na^+ to the cation-binding site induces helix IV movement with an increase in sugar affinity. **[2]** *Inward Na^+- and melibiose-bound state*. Sugar binding from the cytoplasm initiates the locking process (Fig. 6a, b). **[3]** *Occluded Na^+- and melibiose-bound state*. Closure of the cytoplasmic cavity by the hydrophobic patch is locked by L-1 and L-2. **[4]** Outward Na^+- and melibiose-bound state. Interactions at L-3 and L-4 facilitate a conformational transition from the occluded to an outward state. **[5]** Outward melibiose-released state. Bound melibiose is released to the periplasmic side from the open outer gate. The crystal structures of $MelB_{St}$ suggest that the cation exits via the internal cavity that contains the sugar-binding site and that a bound sugar should restrain the dynamics of the bound cation; therefore, release of sugar is a prerequisite for releasing Na^+. The structural basis for the ordered release is supported by kinetic studies[4,11] and the behavior of mutant G117R[9], which catalyzes melibiose exchange but no reaction involving net Na^+ transport, i.e., involving only steps [1] $\Leftrightarrow$ [5]. **[6]** Outward Na^+-released state. Deformation of the cation-binding site facilitates Na^+ release as suggested by the Mol-B structure (Fig. 3b). **[7]** Occluded-empty state. Formation of the unloaded intermediate state occluded on both sides. **[8]** Inward-empty state. Once the cavity is open to the cytoplasm, the next transport cycle begins. Melibiose efflux involves the whole cycle with one sugar and one charge moving across the membrane. In contrast, melibiose exchange involves only states **[1-5]**.

Interestingly, it appears that the kinetic model is similar for different MFS permeases regardless of the coupling cation[35,48,49]. In the solely H^+-coupled LacY[50-53], it is well established that at physiological pH, LacY is protonated[52]. Sugar binds only to protonated LacY[50,53] and dissociates prior to the release of H^+ during symport[50]. The inward-facing crystal structures of LacY[16,17] indicate that the sugar-binding site is coupled with the H^+-binding site through an electrostatic network; as a result, the affinity for the sugar binding is optimized in a protonated state. A similar coupling phenomenon is observed in MelB. The comparison of the structures of Mol-A and Mol-B reveals that a protonated cation-binding site is coupled with a properly formed sugar-binding pocket, and the deformation of the cation-binding site induces deformation of the sugar-binding site. In LacY, the H^+ may involve in a single side chain (eg., Glu325)[16,17,35,54]; in MelB, the H^+ may be bound in different forms, a protonated side chain (eg., Asp59) or as H_3O^+ that is shared by Asp55, Asp59, and Asp124 in the metal-binding cavity. Possibly, these two protonation forms represent different states of bound H^+ in MelB.

What is the effect of Na^+ or Li^+ on MelB? In general, binding of Na^+ or Li^+ requires 4-6 coordination numbers from 2-3 helices, and the small ionic radius of Na^+ and Li^+ require the coordination ligands in closer distance. Thus, metal binding should induce a relatively large change in movement of helices. Based on the structures of $MelB_{St}$, it is anticipated that Na^+ binding recruits Asp124 to complete Na^+ binding, resulting in movement of helix IV with Tyr120 and Trp128 for aromatic stacking with the bound sugar. It is well known that sugar affinity is largely increased by aromatic stacking in LacY[40]. According to this notion, Na^+

and Li^+ are more effective 'activators' than H^+. This structural interpretation is consistent with the previous conclusion derived from functional studies of $MelB_{Ec}$[30,32,38]. Therefore, it is likely that an essential aspect of coupling is that binding of the cation activates the substrate-binding site, a property that is conserved in both MelB and LacY.

What prevents cation leakage in MelB? The opening and closing of the cytoplasmic side to form the substrate exit pathway involves dynamics of cytoplasmic helix V in MelB (Fig. 6a, b), which is initiated only by sugar binding. In the absence of sugar, "the leader", MelB/Na^+ complexes should preferentially populate outward conformations. This structural arrangement can prevent bound Na^+ from futile cycling and also offers an explanation for how the extra-membrane ionic locks, as "the follower", respond to the primary effect of sugar binding in the middle of molecule.

Methods

Large-scale protein production

Full-length $MelB_{St}$ encoded by plasmid pK95 ΔAH/$MelB_{St}$/$CHis_{10}$[4,55] with Leu5→Met and a His_{10}-tag at the C-terminus (namely the WT) was expressed in *E. coli* DW2 strain (*mel*A^+, Δ*mel*B, Δ*lac*ZY)[55]. In a 10-L fermenter, cells were grown in Luria-Bertani (LB) broth supplemented with 50 mM KP_i (pH 7.0), 45 mM $(NH_4)H_2PO_4$, 0.5% glycerol, and 100 mg/L ampicillin at 30 °C until they approached stationary phase at A_{600} of ~3.3. Cells with constitutively overexpressed $MelB_{St}$ were then harvested, resuspended in 20 mM Tris-HCl (pH 7.5), 200 mM NaCl and 10% glycerol, broken with an EmulsiFlex instrument, and centrifuged at 20,000 g for 15 min to remove unbroken cells[56]. Membranes were harvested from the supernatant by ultracentrifugation at $14{,}4651_g$ for 3 h in Beckman rotor, type 45 Ti. The pellets were resuspended in the same buffer, frozen in liquid N_2, and stored at −80 °C. The protein concentration of the membrane samples was assayed using Micro BCA™ Protein Assay Kit (Pierce).

Protein purification

Membranes (14 mg/mL) were extracted with 1.5% n-undecyl-β-D-maltoside (UDM) followed by ultracentrifugation at 265000_g for 30 min. Purification was performed by cobalt-affinity chromatography (TALON resins). The column was pre-equilibrated with 50 mM NaP_i (pH 7.6), 200 mM NaCl, 10% glycerol, 0.035% UDM, 5 mM imidazole. After loading and washing the column with 35 mM imidazole buffer, $MelB_{St}$ was eluted with buffer containing 200 mM imidazole, concentrated with VIVASPIN 20 (50 kDa cutoff), dialyzed twice against 1 L of 20 mM Tris-HCl (pH 7.5), 100 mM NaCl, 10% glycerol, 0.035% UDM, further concentrated to >20 mg/mL, and finally ultracentrifuged at $>360{,}000_g$ for 45 min. The protein was flash-frozen in liquid nitrogen and stored at −80 °C. From a 10-L culture, highly purified $MelB_{St}$ at 30-40 mg was obtained routinely.

ITC

ITC measurements were performed in a nano isothermal titration calorimeter (*TA Instruments*). The purified $MelB_{St}$ in the dialysis buffer was injected into the ITC sample cell, and 6 mM melibiose dissolved in the same dialysis buffer was titrated incrementally

into the protein sample, and the heat rate was recorded at 25 °C. Melibiose binding was also measured in the presence of 100 mM LiCl. The cumulative heat change (ΔQ) was plotted against the molar ratio of melibiose to $MelB_{St}$ and fitted with the one-site independent binding model (*NanoAnalyse software*).

Protein expression for functional studies

E. coli DW2 cells containing a given plasmid were grown in LB broth with 100 mg/L of ampicillin at 37 °C. The overnight cultures were diluted by 5% to LB broth supplemented with 0.5% glycerol and 100 mg/L of ampicillin, and the constitutive overexpression was obtained by shaking at 30 °C for another 5 h.

Preparation of right-side-out (RSO) membrane vesicles

RSO membrane vesicles were prepared from *E. coli* DW2 cells by osmotic lysis[4,57,58]. Cells were incubated with 50 μg/ml lysozyme in the presence of 10 mM EDTA (pH 7.5), 5 mM dithiothreitol (DTT), and 30% (w/v) sucrose for 45 min; the yielded spheroplasts were harvested by centrifugation at 14,000g for 40 min at 4 °C and suspended with 20-mL cocktail containing 100 mM KP_i (pH 7.5), 20 mM $MgSO_4$, 30% sucrose, 5 mM DTT, 1 mg/mL deoxyribonuclease, and 1 mg/mL ribonuclease. The resuspended spheroplasts were lysed by rapid dilution into 1-L 50 mM KP_i (pH 7.5) buffer with 5 mM DTT, and the solution was incubated at 37 °C for 10 min. After further incubation with 10 mM EDTA (pH 7.0) for 10 min and 15 mM $MgSO_4$ for another 10 min, the total membrane vesicles were harvested by centrifugation at $14{,}000_g$ for 25 min at 4 °C. The RSO vesicles were collected from the supernatant after centrifugation at 800_g for 12 min at 4 °C, then extensively washed and resuspended with 100 mM KP_i (pH 7.5) at a protein concentration of about 20-28 mg/ml, frozen in liquid N_2, and stored at − 80 °C.

Melibiose transport assay with intact cells

Melibiose active transport with intact cells were carried out with [1-^{3}H]melibiose[4], which was custom synthesized by *PerkinElmer* (Boston, MA). *E. coli* DW2 cells expressing $MelB_{St}$ were washed with 50 ml of 100 mM KP_i (pH 7.5), so-called Na^+-free buffer. The cell pellets were resuspended with 100 mM KP_i (pH 7.5) and 10 mM $MgSO_4$, adjusted to an A_{420} = 10 (~ 0.7 mg protein/ml), and aliquoted with 50 μl. Transport was initiated by adding 2 μl of [^{3}H]melibiose with a specific activity of 10 mCi/mmol at a final concentration of 0.4 mM in the absence or presence of either 20 mM NaCl or LiCl, and stopped at a given incubation time. Intracellular melibiose was assayed by a fast filtration.

Melibiose efflux and exchange assays

RSO membrane vesicles containing the WT or a mutant $MelB_{St}$ in 100 mM KP_i (pH 7.5) and 10 mM $MgSO_4$ were concentrated to about 28 mg/ml, and pre-equilibrated overnight on ice with 20 mM [^{3}H]melibiose (10 mCi/mmol), 0.75 μM monensin, and 10 μM carbonylcyanide m-chlorophenylhydrazone[4,9,11], without or with 20 mM NaCl or LiCl. Aliquots (2 μl) were diluted 200 fold into a given buffer in the absence (efflux) or presence (exchange) of 20 mM unlabeled melibiose[50], and reactions were terminated by dilution and rapid filtration at a given time.

Western blotting

25 μg of RSO membranes were loaded onto each well of SDS-16% PAGE. After transfer onto the PVDF membrane, $MelB_{St}$ proteins were detected with anti-His tag antibody, and imaged by the ImageQuant™ LAS 4000 Biomolecular Imager (GE Health Care Life Science)[47].

Trp→D^2G FRET

2'-(N-dansyl)aminoalkyl-1-thio-β-D-galactopyranoside (D^2G)[4,9,43,47,59] was used to test affinity for the cosubstrate via FRET from Trp residues to the dansyl moiety of the D^2G bound with $MelB_{St}$. Steady-state fluorescence measurements were performed in a 3-mm quartz cuvette (Hitachi F-7000 Fluorescence Spectrophotomer or AMINCO-Bowman Series 2 Spectrometer).

The purified sugar-free $MelB_{St}$ (1 μM) in the dialysis buffer or the buffer with 100 mM LiCl instead of NaCl was excited at wavelength of 290 nm, and the emission fluorescence was recorded between 415-575 nm. With 10 μM D^2G (the K_D value for the WT[4]), displacement of D^2G bound by $MelB_{St}$ was carried out by adding 50 mM melibiose, methyl-β-D-thiogalactoside (TMG), glucose, or sucrose, respectively. The difference spectra before and after the addition of a given sugar for displacement (ΔI) is calculated and plotted.

The RSO membrane vesicles prepared from DW2 cells expressed $MelB_{St}$ (1 mg/mL)[4,9] in 100 mM KP_i (pH, 7.5) were excited at wavelength of 290 nm, the emission fluorescence at wavelength of 490 nm was recorded for one minute after each following addition unless specified: (1) 10 μM D^2G; (2) 20 mM NaCl or LiCl; (3) 50 mM NaCl or LiCl; (4) 120 mM melibiose or same vulom of water.

Half-maximal displacement of bound D^2G (IC_{50})

Melibiose was added stepwise to the samples containing the RSO vesicles with D^2G (10 μM) and 20 mM NaCl until no change in fluorescence emission occurred. The decrease in fluorescent intensity after each addition was corrected by the water dilution, and plotted as a function of melibiose concentration. The IC_{50} value was determined by fitting a hyperbolic function to the data (*OriginPro*).

Na^+-stimulation constant ($K_{0.5}$) for D^2G FRET

Applying the same experimental setup, NaCl was consecutively added to the sample containing the RSO vesicles and D^2G (10 μM)[9]. An identical volume of water was used for the control. Fluorescent increase [ΔI, the difference before (I_0) and after the addition of NaCl] was expressed as the percentage of the I_0, corrected by a dilution effect, and then plotted as a function of Na^+ concentration. The $K_{0.5}$ for Na^+ simulation was determined by fitting a hyperbolic function to the data (*OriginPro*).

Mutagenesis

All $MelB_{St}$ mutants were constructed with the QuickChange™ Site-Directed Mutagenesis Kits (Stratagene) using the plasmid pK95 ΔAH/$MelB_{St}$/$CHis_{10}$ as the template[4].

Gel filtration chromatography

Gel filtration was performed in a Superdex 200^{TM} 10/300 GL column on a Fast Protein Liquid Chromatography instrument. For the stability studies, the protein sample was placed at 23 °C for 5 days, and analyzed by the gel filtration chromatography and the D^2G FRET assay.

Pre-crystallization phospholipids treatment

Prior to setting up crystallization trials, the protein samples were thawed out from −80 °C, ultracentrifuged at 384,492$_g$ for 45 min at 4 °C (*Beckman Coulter Optima MAX*, TLA-100 rotor), diluted to a final protein concentration of 7 mg/mL, and incubated with phospholipid at a concentration of 3.3 mM (*E. coli* Extract Polar, *Avanti*, #100600) from a 15-mM stocks dissolved with the dialysis buffer.

Crystallization, data collection and processing

Crystallization of $MelB_{St}$ was carried out by the hanging-drop vapor-diffusion method at 23 °C by mixing 2 μL of phospholipid-treated protein samples[60] containing 5 mM αNPG with 2 μL reservoir containing 100 mM MES (pH 6.5), 100 mM NaCl, 50 mM $CaCl_2$, 35-37% PEG 400, and 0.08% octyl-β-D-galactopyranoside. Crystals were frozen with liquid nitrogen and tested for X-ray diffraction at the Lawrence Berkeley National Laboratory, ALS BL 8.2.1, 8.2.2, 5.0.1, 5.0.2 or at the Stanford Synchrotron Radiation Light Source BL 7-1 via remote data collection. The complete diffraction dataset was collected at 100 K from a single cryo-cooled crystal at wavelength of 1.004 Å with an ADSC QUANTUM 315 detector at ALS BL 5.0.2; image data were processed with HKL 2000[61] to a resolution of 3.35 Å with 98 % completeness (Table 1).

Structure solution and refinement

Data were processed in space groups $P3_221$, $P3_121$, $P3_2$ and $P3_1$. The data set was analyzed by Structure Factor Check on CCP4[62] suite and Phenix Xtriage[63,64], which indicated a strong off-origin peak at 0, 0, 0.5 along *c** axis and also revealed merohedral twinning with twin fraction of 0.41 for the data processed in space groups $P3_2$ and $P3_1$. Search probes were prepared using the server I-TASSER[65] using the structures of MFS permeases, the inward LacY (PDB, 2V8N) and GlpT (1PW4), the occluded EmrD (2GFP), as well as the outward FucP (3O7Q). Using Phaser 2.52 program[66] in Phenix suite, a single copy of each threading model with deletion of the longer $loop_{6\text{-}7}$ and $loop_{10\text{-}11}$, and the C-terminal tail was used as the search probe to test the data processed in all space groups. Applying the native Patterson map and omit map to assist the MR processes, a maximal solution from the FucP-based $MelB_{St}$ model was identified, and the crystal symmetry was determined to be $P3_2$ containing two additional pseudo-crystallographic symmetries with 74% solvent content.

The asymmetric unit contains four closely aligned molecules with two types of pseudo-twofold symmetry (twinning) along the *b* axis, with Mol-A and Mol-B related by 172° and Mol-C and Mol-D related by 160° (Supplementary Fig. S3). Mol-AB and Mol-CD are related by 0.5 pseudo-translation. Twin refinement was carried out by REFMAC 5.7

program using the Jelly-Body-Restrained refinement option in CCP4 suite with the twinning operator *k, h, −l*. Initial refinement yielded R/R_{free} of 0.37/0.42. Model verification was done by systematic calculation of omit maps at various regions. With iterative rounds of manual model building followed by simulated annealing and density modification, an interpretable density map to 3.35 Å resolution was obtained allowing assignment of most side chains for Mol-A and Mol-B (Supplementary Figs. S3c,d and S5a,b). Final refinement was carried out using the Tangent Least-Square Jelly-Body Restrained twin refinement, where the R/R_{free} values dropped to 0.30/0.35 (Table 1). Since pseudo-symmetries are present, higher apparent R/R_{free} values are expected[67]. Out of 476 residues, 1-432 in Mol-A, regions 1-210 and 235-450 in Mol-B, 1-431 in Mol-C, as well as 1-100, 109-210, 235-398, and 408-431 in Mol-D, were well resolved. 82.2 % of residues are in most favored, 17.4 % in generously allowed, and 0.4% in disallowed regions. Visualization of omit maps and manual model building were performed using Coot 0.7[68]. Surface electro-potential maps were calculated using APBS software[69]. All crystallographic figures were generated with Pymol 1.5[70].

Supplementary Material

Refer to Web version on PubMed Central for supplementary material.

Acknowledgements

We thank Luis Reuss and R. Bryan Sutton for critical reading of the manuscript and Shailika Nurva, Hariharan Parameswaran, Elena Tikhonova, Gill Verner, and Shushi Nagamori for assistance. We thank Kelsey Markham for constructing most of the mutants. We also thank the staffs at the Advanced Light Source, Lawrence Berkeley National Laboratory and the Stanford Synchrotron Radiation Light Source for assistance with X-ray data collection. The diffraction dataset was collected at ALS BL 5.0.2. This work was supported by the National Science Foundation (grant MCB-1158085 to L.G.) and (grant MCB-0450970 to H.R.K.) and the Norman Hackerman Advanced Research Program (grant 010674-0034-2009 to L.G.), as well as supported by the National Institutes of Health (grants R21HL087895 and R01GM095538 to L.G.) and (grants R01DK051131 and R01DK069463 to H.R.K.).

References

1. Poolman B, et al. Cation and sugar selectivity determinants in a novel family of transport proteins. Molecular microbiology. 1996; 19:911–922. [PubMed: 8830272]
2. Saier MH Jr. Families of transmembrane sugar transport proteins. Molecular microbiology. 2000; 35:699–710. [PubMed: 10692148]
3. Mizushima K, et al. Cloning and sequencing of the *melB* gene encoding the melibiose permease of *Salmonella typhimurium LT2*. Mol Gen Genet. 1992; 234:74–80. [PubMed: 1495487]
4. Guan L, Nurva S, Ankeshwarapu SP. Mechanism of melibiose/cation symport of the melibiose permease of *Salmonella typhimurium*. J Biol Chem. 2011; 286:6367–6374. [PubMed: 21148559]
5. Reiling JH, et al. A haploid genetic screen identifies the major facilitator domain containing 2A (MFSD2A) transporter as a key mediator in the response to tunicamycin. Proc Natl Acad Sci U S A. 2011; 108:11756–11765. [PubMed: 21677192]
6. Saier MH Jr. et al. The major facilitator superfamily. Journal of molecular microbiology and biotechnology. 1999; 1:257–279. [PubMed: 10943556]
7. Wilson TH, Ding PZ. Sodium-substrate cotransport in bacteria. Biochim Biophys Acta. 2001; 1505:121–130. [PubMed: 11248194]
8. Wilson DM, Wilson TH. Cation specificity for sugar substrates of the melibiose carrier in *Escherichia coli*. Biochim Biophys Acta. 1987; 904:191–200. [PubMed: 3311166]

9. Guan L, Jakkula SV, Hodkoff AA, Su Y. Role of Gly117 in the cation/melibiose symport of MelB of *Salmonella typhimurium*. Biochemistry. 2012; 51:2950–2957. [PubMed: 22413840]
10. Niiya S, Moriyama Y, Futai M, Tsuchiya T. Cation coupling to melibiose transport in *Salmonella typhimurium*. Journal of bacteriology. 1980; 144:192–199. [PubMed: 6998948]
11. Bassilana M, Pourcher T, Leblanc G. Facilitated diffusion properties of melibiose permease in *Escherichia coli* membrane vesicles. Release of co-substrates is rate limiting for permease cycling. J Biol Chem. 1987; 262:16865–16870. [PubMed: 3316227]
12. Bassilana M, Pourcher T, Leblanc G. Melibiose permease of *Escherichia coli*. Characteristics of co-substrates release during facilitated diffusion reactions. J Biol Chem. 1988; 263:9663–9667. [PubMed: 2838475]
13. Damiano-Forano E, Bassilana M, Leblanc G. Sugar binding properties of the melibiose permease in *Escherichia coli* membrane vesicles. Effects of Na^+ and H^+ concentrations. J Biol Chem. 1986; 261:6893–6899. [PubMed: 3516999]
14. Mus-Veteau I, Pourcher T, Leblanc G. Melibiose permease of *Escherichia coli*: substrate-induced conformational changes monitored by tryptophan fluorescence spectroscopy. Biochemistry. 1995; 34:6775–6783. [PubMed: 7756309]
15. Yousef MS, Guan L. A 3D structure model of the melibiose permease of *Escherichia coli* represents a distinctive fold for Na^+ symporters. Proc Natl Acad Sci U S A. 2009; 106:15291–15296. [PubMed: 19706416]
16. Abramson J, et al. Structure and mechanism of the lactose permease of *Escherichia coli*. Science. 2003; 301:610–615. [PubMed: 12893935]
17. Guan L, Mirza O, Verner G, Iwata S, Kaback HR. Structural determination of wild-type lactose permease. Proc Natl Acad Sci U S A. 2007; 104:15294–15298. [PubMed: 17881559]
18. Huang Y, Lemieux MJ, Song J, Auer M, Wang DN. Structure and mechanism of the glycerol-3-phosphate transporter from *Escherichia coli*. Science. 2003; 301:616–620. [PubMed: 12893936]
19. Yin Y, He X, Szewczyk P, Nguyen T, Chang G. Structure of the multidrug transporter EmrD from *Escherichia coli*. Science. 2006; 312:741–744. [PubMed: 16675700]
20. Dang S, et al. Structure of a fucose transporter in an outward-open conformation. Nature. 2010; 467:734–738. [PubMed: 20877283]
21. Sun L, et al. Crystal structure of a bacterial homologue of glucose transporters GLUT1-4. Nature. 2012; 490:361–366. [PubMed: 23075985]
22. Pedersen BP, et al. Crystal structure of a eukaryotic phosphate transporter. Nature. 2013; 496:533–536. [PubMed: 23542591]
23. Newstead S, et al. Crystal structure of a prokaryotic homologue of the mammalian oligopeptide-proton symporters, PepT1 and PepT2. The EMBO journal. 2011; 30:417–426. [PubMed: 21131908]
24. Purhonen P, Lundback AK, Lemonnier R, Leblanc G, Hebert H. Three-dimensional structure of the sugar symporter melibiose permease from cryo-electron microscopy. J Struct Biol. 2005; 152:76–83. [PubMed: 16139519]
25. Madej MG, Dang S, Yan N, Kaback HR. Evolutionary mix-and-match with MFS transporters. Proc Natl Acad Sci U S A. 2013; 110:5870–5874. [PubMed: 23530251]
26. Yamashita A, Singh SK, Kawate T, Jin Y, Gouaux E. Crystal structure of a bacterial homologue of Na^+/Cl^--dependent neurotransmitter transporters. Nature. 2005; 437:215–223. [PubMed: 16041361]
27. Kovalevsky AY, et al. Identification of the elusive hydronium ion exchanging roles with a proton in an enzyme at lower pH values. Angew Chem Int Ed Engl. 2011; 50:7520–7523. [PubMed: 21604345]
28. Zani ML, Pourcher T, Leblanc G. Mutagenesis of acidic residues in putative membrane-spanning segments of the melibiose permease of *Escherichia coli*. II. Effect on cationic selectivity and coupling properties. J Biol Chem. 1993; 268:3216–3221. [PubMed: 8428998]
29. Pourcher T, Zani ML, Leblanc G. Mutagenesis of acidic residues in putative membrane-spanning segments of the melibiose permease of *Escherichia coli*. I. Effect on Na(+)-dependent transport and binding properties. J Biol Chem. 1993; 268:3209–3215. [PubMed: 8428997]

30. Granell M, Leon X, Leblanc G, Padros E, Lorenz-Fonfria VA. Structural insights into the activation mechanism of melibiose permease by sodium binding. Proc Natl Acad Sci U S A. 2010; 107:22078–22083. [PubMed: 21135207]
31. Bas DC, Rogers DM, Jensen JH. Very fast prediction and rationalization of pKa values for protein-ligand complexes. Proteins. 2008; 73:765–783. [PubMed: 18498103]
32. Pourcher T, Bassilana M, Sarkar HK, Kaback HR, Leblanc G. The melibiose/Na^+ symporter of *Escherichia coli*: kinetic and molecular properties. Philosophical transactions of the Royal Society of London. Series B, Biological sciences. 1990; 326:411–423. [PubMed: 1970646]
33. Faham S, et al. The crystal structure of a sodium galactose transporter reveals mechanistic insights into Na^+/sugar symport. Science. 2008; 321:810–814. [PubMed: 18599740]
34. Ressl S, Terwisscha van Scheltinga AC, Vonrhein C, Ott V, Ziegler C. Molecular basis of transport and regulation in the Na(+)/betaine symporter BetP. Nature. 2009; 458:47–52. [PubMed: 19262666]
35. Guan L, Kaback HR. Lessons from lactose permease. Annu Rev Biophys Biomol Struct. 2006; 35:67–91. [PubMed: 16689628]
36. Guan L, Sahin-Toth M, Kaback HR. Changing the lactose permease of *Escherichia coli* into a galactose-specific symporter. Proc Natl Acad Sci U S A. 2002; 99:6613–6618. [PubMed: 12011425]
37. Guan L, Sahin-Toth M, Kalai T, Hideg K, Kaback HR. Probing the mechanism of a membrane transport protein with affinity inactivators. J Biol Chem. 2003; 278:10641–10648. [PubMed: 12471022]
38. Cordat E, Leblanc G, Mus-Veteau I. Evidence for a role of helix IV in connecting cation- and sugar-binding sites of *Escherichia coli* melibiose permease. Biochemistry. 2000; 39:4493–4499. [PubMed: 10757998]
39. Zani ML, Pourcher T, Leblanc G. Mutation of polar and charged residues in the hydrophobic NH2-terminal domains of the melibiose permease of *Escherichia coli*. J Biol Chem. 1994; 269:24883–24889. [PubMed: 7929169]
40. Guan L, Hu Y, Kaback HR. Aromatic stacking in the sugar binding site of the lactose permease. Biochemistry. 2003; 42:1377–1382. [PubMed: 12578349]
41. Vazquez-Ibar JL, Guan L, Svrakic M, Kaback HR. Exploiting luminescence spectroscopy to elucidate the interaction between sugar and a tryptophan residue in the lactose permease of *Escherichia coli*. Proc Natl Acad Sci U S A. 2003; 100:12706–12711. [PubMed: 14566061]
42. Meyer-Lipp K, et al. The inner interhelix loop 4-5 of the melibiose permease from *Escherichia coli* takes part in conformational changes after sugar binding. J Biol Chem. 2006; 281:25882–25892. [PubMed: 16822867]
43. Maehrel C, Cordat E, Mus-Veteau I, Leblanc G. Structural studies of the melibiose permease of *Escherichia coli* by fluorescence resonance energy transfer. I. Evidence for ion-induced conformational change. J Biol Chem. 1998; 273:33192–33197. [PubMed: 9837887]
44. Quistgaard EM, Low C, Moberg P, Tresaugues L, Nordlund P. Structural basis for substrate transport in the GLUT-homology family of monosaccharide transporters. Nature structural & molecular biology. 2013; 20:766–768.
45. Yan H, et al. Structure and mechanism of a nitrate transporter. Cell reports. 2013; 3:716–723. [PubMed: 23523348]
46. Zheng H, Wisedchaisri G, Gonen T. Crystal structure of a nitrate/nitrite exchanger. Nature. 2013; 497:647–651. [PubMed: 23665960]
47. Jakkula SV, Guan L. Reduced Na^+ affinity increases turnover of Salmonella enterica serovar Typhimurium MelB. Journal of bacteriology. 2012; 194:5538–5544. [PubMed: 22865849]
48. Doki S, et al. Structural basis for dynamic mechanism of proton-coupled symport by the peptide transporter POT. Proc Natl Acad Sci U S A. 2013; 110:11343–11348. [PubMed: 23798427]
49. Madej MG, Soro SN, Kaback HR. Apo-intermediate in the transport cycle of lactose permease (LacY). Proc Natl Acad Sci U S A. 2012; 109:E2970–2978. [PubMed: 23012238]
50. Kaczorowski GJ, Kaback HR. Mechanism of lactose translocation in membrane vesicles from *Escherichia coli*. 1. Effect of pH on efflux, exchange, and counterflow. Biochemistry. 1979; 18:3691–3697. [PubMed: 38836]

51. Smirnova I, Kasho V, Sugihara J, Choe JY, Kaback HR. Residues in the H^+ translocation site define the pKa for sugar binding to LacY. Biochemistry. 2009; 48:8852–8860. [PubMed: 19689129]
52. Smirnova IN, Kasho V, Kaback HR. Protonation and sugar binding to LacY. Proc Natl Acad Sci U S A. 2008; 105:8896–8901. [PubMed: 18567672]
53. Smirnova I, Kasho V, Sugihara J, Vazquez-Ibar JL, Kaback HR. Role of protons in sugar binding to LacY. Proc Natl Acad Sci U S A. 2012; 109:16835–16840. [PubMed: 23033496]
54. Carrasco N, et al. Characterization of site-directed mutants in the *lac* permease of *Escherichia coli*. 2. Glutamate-325 replacements. Biochemistry. 1989; 28:2533–2539. [PubMed: 2567181]
55. Pourcher T, Leclercq S, Brandolin G, Leblanc G. Melibiose permease of *Escherichia coli*: large scale purification and evidence that H^+, Na^+, and Li^+ sugar symport is catalyzed by a single polypeptide. Biochemistry. 1995; 34:4412–4420. [PubMed: 7703254]
56. Chae PS, et al. Maltose-neopentyl glycol (MNG) amphiphiles for solubilization, stabilization and crystallization of membrane proteins. Nat Methods. 2010; 7:1003–1008. [PubMed: 21037590]
57. Kaback, HR.; Colowick, Nathan P. Methods in Enzymol. Kaplan, Nathan P.; Jakoby, William B., editors. Vol. XXII. Elsevier; 1971. p. 99-120.
58. Short SA, Kaback HR, Kohn LD. D-lactate dehydrogenase binding in *Escherichia coli* dld- membrane vesicles reconstituted for active transport. Proc Natl Acad Sci USA. 1974; 71:1461–1465. [PubMed: 4598306]
59. Cordat E, Mus-Veteau I, Leblanc G. Structural studies of the melibiose permease of *Escherichia coli* by fluorescence resonance energy transfer. II. Identification of the tryptophan residues acting as energy donors. J Biol Chem. 1998; 273:33198–33202. [PubMed: 9837888]
60. Guan L, Smirnova IN, Verner G, Nagamori S, Kaback HR. Manipulating phospholipids for crystallization of a membrane transport protein. Proc Natl Acad Sci U S A. 2006; 103:1723–1726. [PubMed: 16446422]
61. Otwinowski, Z.; Minor, W. Macromolecular Crystallography, part A. Vol. 276. Academic Press; 1997. Method Enzymol; p. 307-326.
62. Winn MD, et al. Overview of the CCP4 suite and current developments. Acta crystallographica. Section D, Biological crystallography. 2011; 67:235–242.
63. Adams PD, et al. PHENIX: a comprehensive Python-based system for macromolecular structure solution. Acta crystallographica. Section D, Biological crystallography. 2010; 66:213–221.
64. Padilla JE, Yeates TO. A statistic for local intensity differences: robustness to anisotropy and pseudo-centering and utility for detecting twinning. Acta crystallographica. Section D, Biological crystallography. 2003; 59:1124–1130.
65. Zhang Y. I-TASSER server for protein 3D structure prediction. BMC bioinformatics. 2008; 9:40. [PubMed: 18215316]
66. McCoy AJ, et al. Phaser crystallographic software. Journal of applied crystallography. 2007; 40:658–674. [PubMed: 19461840]
67. Lee S, Sawaya MR, Eisenberg D. Structure of superoxide dismutase from Pyrobaculum aerophilum presents a challenging case in molecular replacement with multiple molecules, pseudo-symmetry and twinning. Acta crystallographica. Section D, Biological crystallography. 2003; 59:2191–2199.
68. Emsley P, Lohkamp B, Scott WG, Cowtan K. Features and development of Coot. Acta crystallographica. Section D, Biological crystallography. 2010; 66:486–501.
69. Baker NA, Sept D, Joseph S, Holst MJ, McCammon JA. Electrostatics of nanosystems: application to microtubules and the ribosome. Proc Natl Acad Sci U S A. 2001; 98:10037–10041. [PubMed: 11517324]
70. Schrodinger, L. The PyMOL Molecular Graphics System. 2013. Version 1.5

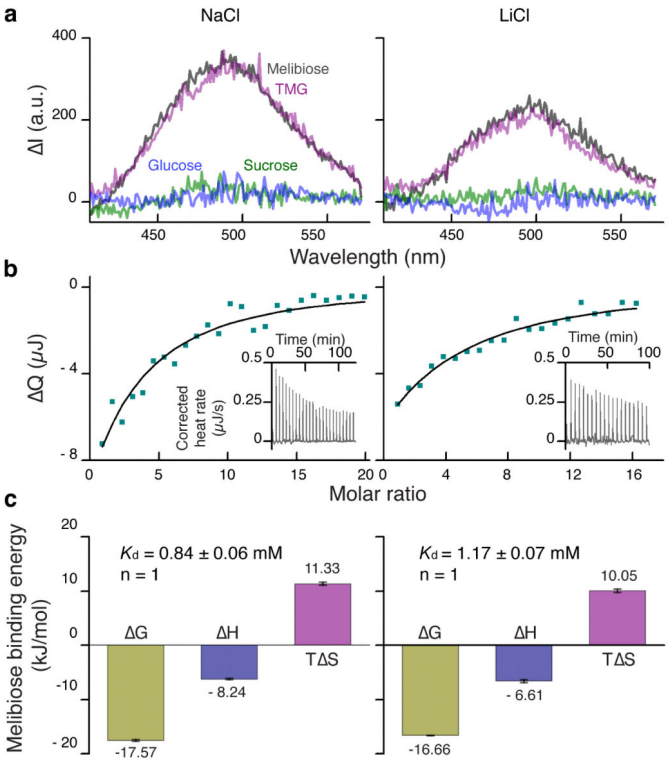

Figure 1. Functional characterization

Purified $MelB_{St}$ containing 100 mM NaCl or LiCl were subjected to D^2G FRET and ITC measurements. **a**, D^2G FRET measurement. With an excitation wavelength of 290 nm, emission spectra were collected between 415-575 nm. Difference spectra (ΔI) were calculated before and after addition of a given sugar (50 mM). Gray curves, melibiose; purple curves, TMG; green curves, sucrose curves; blue curves, glucose. **b**, ITC measurement. Melibiose titration thermograms (insets) were recorded at 25 °C. Cumulative heat change (ΔQ) is plotted as function of the molar ratio of melibiose/$MelB_{St}$, and fitted with the one-site Independent Binding Model. **c**, Melibiose binding energetics. Enthalpy change (ΔH) and the association constant (K_a) were measured directly; dissociation constant $K_d = 1/K_a$; free energy change $\Delta G = -RT \ln K_a$; entropy change $\Delta TS = \Delta H - \Delta G$. n, stoichiometry. Error bar, s.d., n = 2.

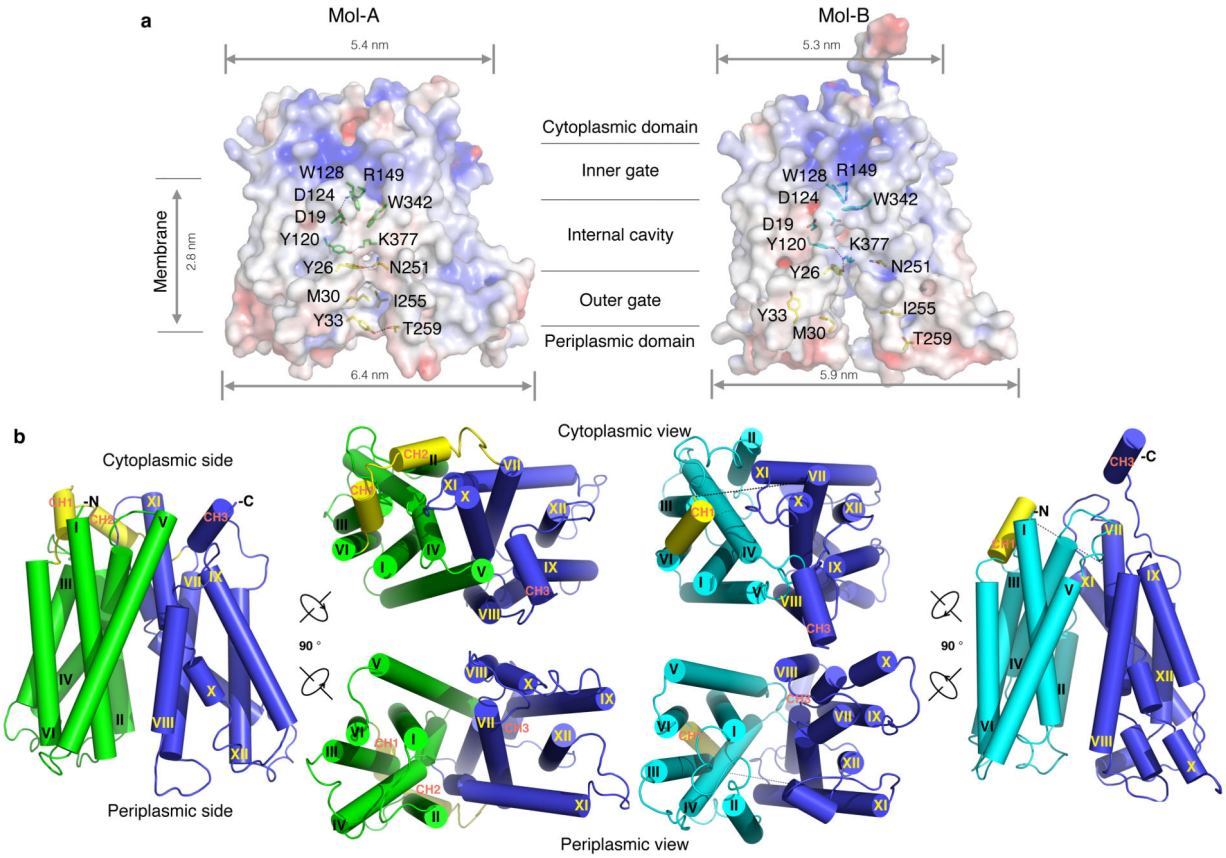

Figure 2. Crystal structures of $MelB_{St}$ in two outward conformations

a, Surface electro-potential maps with side-chains forming the outer gate and the internal cavity shown in yellow and green (Mol-A) or cyan (Mol-B) sticks. **b**, Overall structure of $MelB_{St}$. The N-terminal domains of Mol-A or Mol-B are shown in green and cyan, respectively, and the central loops are shown in yellow. The helices are labeled with Roman numerals. $CH_{1\text{-}3}$ denote the helices in the cytoplasmic loops and the C-terminal tail. All figures showing MelB structures were prepared by $C\alpha^{1\text{-}430}$ superposition of Mol-B on Mol-A.

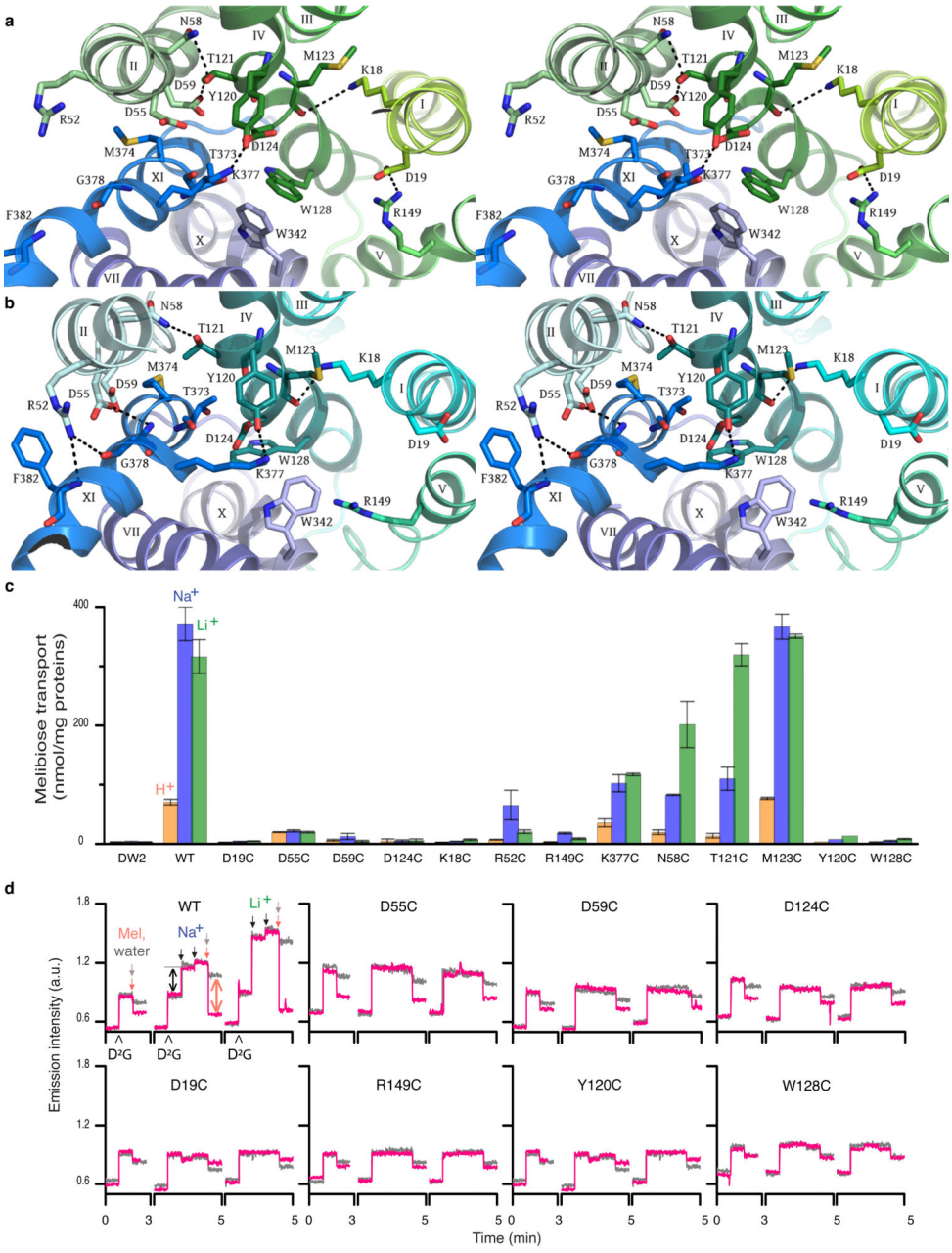

Figure 3. Co-substrate-binding sites

a, Wall-eyed stereo view from the periplasmic side of the internal cavity in Mol-A with the N- and C-halves in green and blue, respectively. **b**, Identical view of Mol-B with N- and C-halves in cyan and blue, respectively. **c**, Steady-state levels of [^{3}H]melibiose accumulation by intact cells at 10 min presented as histograms. DW2, cells without MelB. Error bar, s.e.m.; n = 2 for all mutants with a single-site mutation, and n = 10 for the WT and DW2. **d**, Trp→D^{2}G FRET with RSO vesicles. The emission signals were collected at wavelength of 490 nm after excited at wavelength of 290 nm. Λ, adding 10 μM D^{2}G; pink arrows ↓ adding 120 mM melibiose; gray arrows ↓ adding water; black arrows ↓, adding 20 mM or 50 mM

Na^+ or Li^+. Black double-headed arrows ↔, Na^+ or Li^+ stimulation; pink double-headed arrows ↔, melibiose displacement of D^2G.

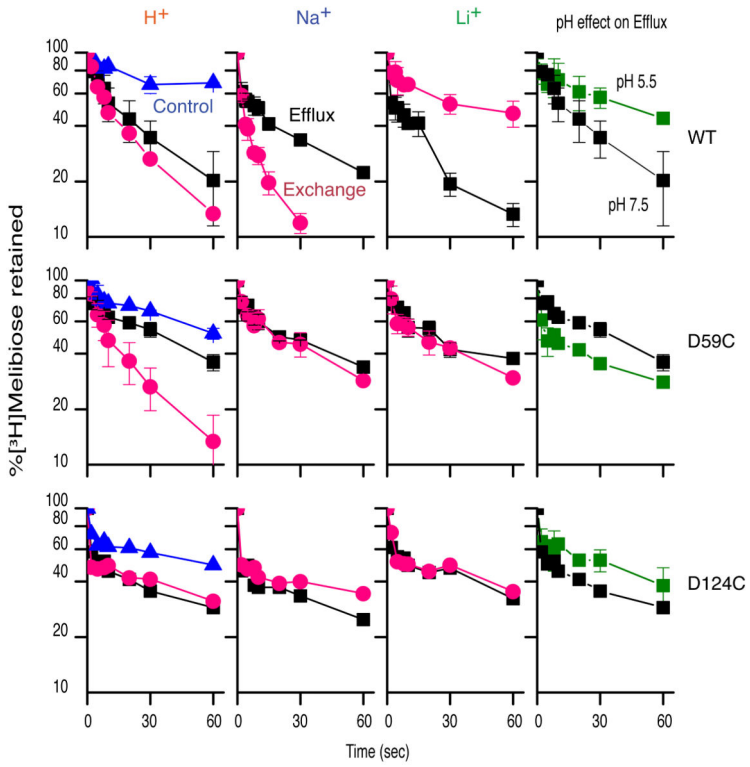

Figure 4. Melibiose efflux and exchange

RSO membrane vesicles (28 mg/ml) containing $MelB_{St}$ were tested for outwardly directed flow of [^{3}H]melibiose in the absence (efflux, squares) or presence (exchange, red circles) of equimolar concentration of unlabeled melibiose. The same experiment was performed in the presence of 20 mM NaCl or LiCl. 2-(4'-maleimidylanilino)naphthalene-6-sulfonic acid (MIANS)-treated vesicles were used for the negative control (blue triangles). Acidic pH effect on melibiose efflux was tested by decreasing the dilution buffer pH to 5.5 (green squares). Error bar, s.e.m., n = 2.

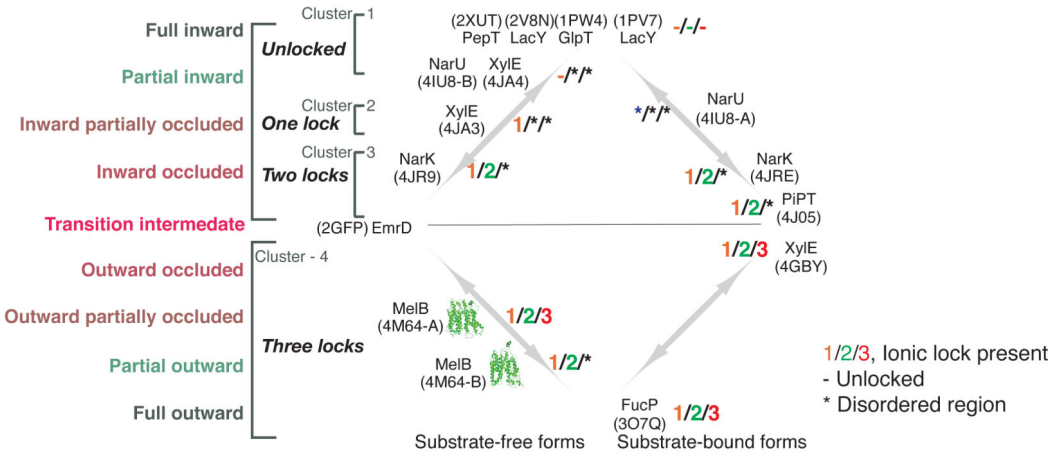

Figure 5. Clusters of MFS permeases in different conformations

Structures were categorized into clusters according to their conformational state. *, disordered region in structure; "-", at an unlocked state; "1/2/3", the presence of lock-1, lock-2, or lock-3. PDB ID is shown for each structure.

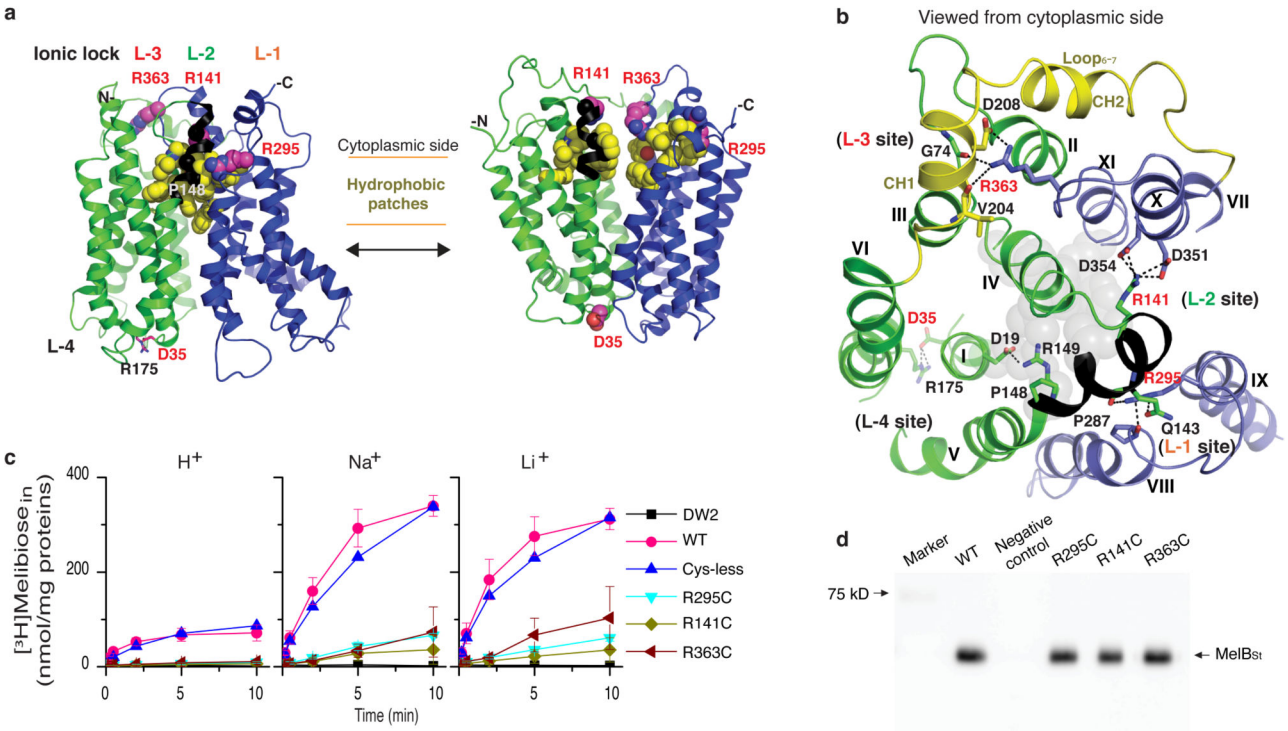

Figure 6. Ionic locks and conformational cycling

N- and C-terminal domains are shown in green and blue, respectively, and hydrophobic patches are in yellow. Arg141-Arg149 stretch is colored as black. "L" denotes positions of ionic locks. **a**, Left, outward partially occluded conformation (Mol-A); right, threading model for inward conformation. **b**, Residues forming ionic locks are shown in sticks connected by broken lines. Gray spheres represent the residues involved in sugar binding. **c**, Cys mutant of Arg residue at position 295, 141, or 363. Intact *E. coli* DW2 cells containing WT $MelB_{St}$ or a given mutant were assayed for [^{3}H]melibiose transport (0.4 mM, 10 mCi/mmol) in the absence or presence of 20 mM NaCl or LiCl. Intracellular melibiose expressed as nmol/mg of total proteins is plotted as a function of time. Each single-site mutation is in the WT background. Error bar, s.e.m., n = 2 for the mutants and n = 3 for the WT. **d**, Western blotting. 25 μg of RSO vesicles was loaded on each well and detected by anti-His-tag antibody.

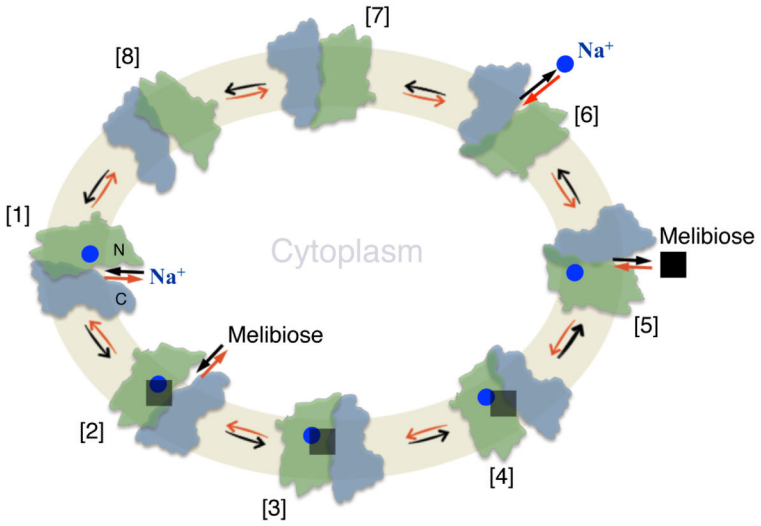

Figure 7. Scheme for Na^+/melibiose symport

[1] – [8] represent kinetic steps in the overall transport cycle. The green color-filled cycle represents the cell inner membrane. Na^+, blue circles; melibiose, black squares. N, the N-terminal domain in green color; C, the C-terminal domain in blue color. Melibiose influx down a sugar concentration gradient starts at step [6] and proceeds via the red arrows around the circle, and melibiose efflux down a sugar concentration gradient starts at [1] proceeds via the black arrows around the circle. Active transport of melibiose against a concentration gradient proceeds from step [6] via the red arrows as the melibiose influx.

Table 1

Data collection and refinement statistics (molecular replacement)

	$MelB_{St}$
Data collection	ALS 5.0.2
Space group	$P3_2$
Cell dimensions□□	
a = *b*, *c* (Å)	127.20, 206.30
γ (°)	120.00
Resolution (Å)	40.00 - 3.35 (3.47 - 3.35)*
R_{sym} or R_{merge}	0.092 (0.77)
$I / \sigma I$	6.0 (1.52)
Completeness (%)	99.4 (99.4)
Redundancy	2.8 (2.7)
Refinement	
Resolution (Å)	38.0 - 3.35 (3.44 - 3.35)
No. reflections	50526
R_{work} / R_{free}	0.30 / 0.35
No. atoms	
Protein	12963
B-factors	
Protein	86.0
R.m.s. deviations	
Bond lengths (Å)	0.012
Bond angles (°)	1.7

*Values in parentheses are for highest-resolution shell.

Table 2

Affinity for melibiose and Na^+

	Melibiose displacement of D^2G IC_{50} (mM)	**Na^+ activation constant for D2G FRET $K_{0.5}$ (mM)**
WT $MelB_{St}$	2.65 ± 0.80[#]	1.92 ± 0.78
R295C	4.04 ± 0.42	3.22 ± 1.07
R141C	5.93 ± 1.61	4.77 ± 0.39
R363C	2.83 ± 0.57	5.51 ± 1.07

[#] s.e.m., n = 2.